Interfacial interactions between DNA and polysaccharide-coated magnetic nanoparticles: insight from simulations and experiments

Maria Psarrou[1,2], Maria Vamvakaki[1,2],

Kostas Karatasos[3], Anastassia N. Rissanou[4,*]

1. Department of Materials Science and Technology, University of Crete, 700 13 Heraklion, Crete, Greece.
2. Institute of Electronic Structure and Laser, FORTH, 700 13 Heraklion, Crete, Greece.
3. Department of Chemical Engineering, University of Thessaloniki, P.O. BOX 420, 54124 Thessaloniki, Greece.
4. Theoretical & Physical Chemistry Institute, National Hellenic Research Foundation, 48 Vassileos Constantinou Avenue, 11635 Athens, Greece.

Correspondence to: trissanou@eie.gr

Abstract

In this work we examine the structural and energetic stability and the interactions between dextran-coated magnetic nanoparticles and a DNA oligonucleotide at ionic strength conditions that are relevant to physiological gene delivery processes. All-atom Molecular Dynamics simulations provided information at the atomic-level regarding the mechanisms responsible for the physical adsorption of Dextran on the magnetic surface and the conditions under which a successful DNA-Dextran complexation can be accomplished. Coulombic interactions were found to play the main role for the formation of the Dextran interfacial layer onto the magnetic surface while hydrogen bonding between the Dextran molecules enhanced the structural integrity of this layer. The Dextran-DNA complexation was also driven by electrostatic interactions between the two moieties. An increase of the salt concentration was found to promote DNA complexation with the

DX-coated magnetic nanoparticles, through the modification of the Coulombic interactions between the DX and DNA chains, which worked synergistically with the increase in hydrogen bonding between the two macromolecules. Comparison of the behavior of the coated with uncoated magnetic nanoparticles, highlighted the significant role of the DX interfacial layer on the DNA association to the magnetic surface. Relevant experimental results provided complementary information for the coated nanoparticle/DNA interactions at different (larger) length scales. A good qualitative agreement was found between the simulation and experimental findings. This study demonstrates that tailoring the nanoparticle coating and ionic strength can optimize the delivery of DNA by fine-tuning the favorable interfacial forces and thus the DNA/MNP binding stability.

Keywords: Interfacial interactions**,** magnetic nanoparticles, polysaccharides, polymer coated particles, gene delivery**,** molecular dynamics simulations

1. Introduction

Gene therapy has been extensively investigated for the treatment of various rare diseases including cancer, heart diseases, and AIDS and harbors great potential towards clinical translation.[1-2] Gene therapy uses nucleic acids, such as DNA and RNA, to modify the genetic material of the diseased cells and is considered as a more effective platform, compared to small molecule drug therapies or protein/enzyme replacement approaches, for the treatment of serious illnesses.[3] Despite the great advantages of nucleic acid-based nanotherapeutics, the effective delivery of genes into the targeted cells still remains a major challenge. The highly polar and negatively charged nucleotides cannot effectively penetrate the hydrophobic bilayer of the cell membrane leading to inefficient gene transfection and poor protein production. To address this issue, various viral and non-viral nanocarriers have been utilized to complex and compact the genetic material, while simultaneously offering protection against hydrolysis and enzymatic degradation, securing its effective transport into the cytosolic area.[2]

Some of the most common non-viral gene vectors rely on the use of cationic polymers such as poly(ethylene imine),[4-5] poly(beta amino esters),[6] poly(amido amine) dendrimers,[7] poly(2-(dimethylamino)ethyl methacrylate and chitosan.[8-10] However, a major drawback of synthetic

cationic polymer nanoparticles is the increased cytotoxicity even at low concentrations, which hinders their potential usage in clinical applications. Recently, there is a growing interest in the development and utilization of hybrid nanoparticle (NP)-based gene carriers, which can combine two highly desirable modalities, i.e., imaging capabilities and gene transport.[11-12] In this context, inorganic nanoparticles, such as gold, silica and iron oxide, coated with a variety of organic molecules, including lipids, polymers and peptides, have been investigated as gene carriers, and have exhibited promising results regarding their cellular uptake.[13-15] NP-assisted DNA delivery offers a number of advantages over traditional DNA delivery methods, such as lipofection and electroporation. It is usually more efficient, less toxic, and more versatile, since it can be used to deliver DNA into a wide range of cell types, including difficult-to-transfect cells such as primary cells and stem cells.[3]

Among the different methods of NP-assisted DNA delivery, magnetofection has recently been used to drive DNA-loaded magnetic nanoparticles (MNPs) in the targeted cells.[16-17] In such processes, the MNPs are usually coated with a variety of functional organic compounds offering additional advantages to the nanocarriers.[18-19] Organic-coated NPs often possess improved colloidal stability, better bioavailability and stealth properties, and may offer other useful functionalities such as antimicrobial action and additional drug/gene binding sites.[20-21] MNPs offer several advantages over other DNA delivery systems, such as viruses and liposomes, since they can be engineered to be biocompatible, non-toxic and can be easily functionalized with targeting ligands and other molecules that bind to specific receptors on the cell surface.[22]

Among the different nanoparticle coatings, polysaccharides which are abundant in nature and possess many desirable properties, such as biodegradability, non-toxicity, and low immunogenicity, have been employed to improve the biocompatibility and stealth properties of colloidal particles.[23-25] Moreover, polysaccharides provide a functional substrate for the attachment of other active molecules, such as targeting ligands, drugs or genes, and facilitate the controlled release of the therapeutic agents from the MNPs. Chitosan, hyaluronic acid and dextran (DX) are the most commonly used polysaccharides to coat the MNPs.[26-28] In particular, DX has attracted significant attention due to its high water solubility, biosafety, biodegradability and facile modification.[29-33] Medarorova et al., presented the development of DX-coated iron oxide NPs for oligonucleotide delivery aiming at the effective microRNA (miRNA) inhibition in tumor cells.[34] The authors examined three different conjugation approaches of the oligonucleotide onto

DX, by varying the length of the spacer (short *vs* long) and the chemistry (degradable *vs* non-degradable groups) linking the oligonucleotide onto the polysaccharide. They concluded that the NPs with the longer spacer formed large agglomerates, leading to negligible cellular uptake, while the NPs with the shorter spacer exhibited enhanced uptake. Moreover, the NPs with the degradable linker exhibited more efficient miRNA inhibition.

Despite the use of DX-functionalized MNPs in gene delivery applications, the microscopic mechanisms underlying their interactions with the nucleotides have not been adequately explored to date. Understanding of these mechanisms will allow optimization of the nanocarriers in terms of their ability to bind and release genetic material and may significantly improve their performance towards a successful gene-delivery process. At the stage of binding, simulation studies can play a valuable role in providing a detailed account regarding the interactions between the nucleotides and the polysaccharide coated MNPs. On this basis, the present work aims at combining atomistically-detailed simulations with an experimental study on DNA complexed with DX-coated MNPs, to provide new insight on the conditions under which such systems can form stable complexes for use in gene-delivery. To the best of our knowledge, neither solely computational studies nor computational/experimental combined efforts have been presented so far on such systems in the literature. In 2011, Wang Z. et al., examined the dynamic behavior of end-tethered single stranded DNA (ssDNA) probes on a silica surface using a hydroxyl-capped linker, in an aqueous solution at the atomic level.[35] The results obtained by molecular dynamics simulations, highlighted the effect of the packing density on the structure and dynamics of ssDNA, providing useful information regarding the behavior of the gene on the silica surface. Another molecular dynamics study suggests that ssDNA molecules arrange in a structured pattern when they attach to carbon nanotubes.[36] The sugar-nucleic acid interactions have been also investigated by various studies in the literature.[37-39] Most of them, summarize that electrostatic charge-charge interactions and hydrogen bonding between sugars/carbohydrates and nucleotides, are the most important types of interaction. However, it is also stated that aromatic π-π, CH/π and hydrophobic interactions can play a significant role in the binding mode of natural carbohydrates with nucleic acids.[40] For example, Lucas R. et al., explored the interactions between carbohydrate-DNA using a dangling-end DNA model consisting of carbohydrate-DNA conjugates where different mono- and disaccharides are attached to the 50-end of the DNA strands and they concluded that stacking has significant role in the formation of sugar-DNA complexes.[37] In

another study by Asensio L. et al., it was reported that the stacking interactions between aminoglycosides and RNA, where several amino groups are protonated, might be reduced with respect to that usually observed for neutral oligosaccharides.[39]

In the current study we examine the structural and energetic stability of the complexes formed between uncoated and DX-coated MNPs and a DNA analogue, at ionic strength conditions relevant to the physiological conditions during the gene delivery process. Atomic-level analysis provided information on the conformational characterization of the DNA strands near the uncoated and coated magnetic surface, on the characteristics of the interfacial layer and on the nature of the dominant interfacial interactions. Comparison of the behavior of the coated and uncoated MNPs, highlighted the role of the DX interfacial layer on DNA binding and allowed an assessment of the required properties of the MNP coating layer for the preparation of robust DNA vehicles facilitating the gene delivery process. The experimental results attested on the validity of the simulation models and provided additional information about the binding efficiency of the DNA molecules onto the surface of DX-coated MNPs and the stability of the hybrid complexes at different (larger) length scales. The simulations successfully captured the qualitative behavior seen in the experiments.

2. Materials and Methods

2.1 Materials. DX (M_n = 40,000 g mol^{-1}) was obtained from Serva and iron (III) oxide, MNPs (NanoArc) with a diameter between 20 and 40 nm, were purchased from Alfa Aesar. Deoxyribonucleic acid sodium salt (DNA) from Calf Thymus, type 1, fibers (58.1 %moles adenine-thymine pair and 41.9 %moles guanine-cytosine pair) (Sigma Aldrich, CAS Number 73049-39-5) and SYBR® Green I Nucleic Acid Gel Stain were purchased from Sigma-Alrich. NaCl (≥99.5%) was obtained from Fluka. Milli-Q water, with a resistivity of 18.2 MΩ•cm at 298 K, was obtained from a Millipore apparatus and was used for the preparation of all samples.

2.2 Synthesis of the DX-coated iron oxide MNPs. DX (0.5 g) was dissolved in milli–Q water at a concentration of 10 mg mL^{-1}. The polymer solution was stirred at 30 °C until complete dissolution. Then, the iron oxide NPs (0.1 g) were added to the polymer solution. The reaction flask was placed in a sonication bath for 15 min before being left under vigorous stirring for 24 h at 30 °C. Finally, the DX-coated NPs were purified to remove the free polymer via 10

centrifugation/redispersion cycles. For each purification cycle, the DX-MNPs were dispersed in 20 mL water and were sonicated in an ultrasound bath for 10 min prior to centrifugation. The product was freeze dried and stored under a N_2 atmosphere until use.

2.3 Preparation of DNA-loaded DX-coated MNPs. The DX-coated MNPs were dispersed in water at a concentration of 3 mg mL^{-1}. Then, 3 μL of the DNA solution (10 ng μL^{-1}) were added to the nanoparticle dispersion. The mixture was left under stirring for 45 min at 4 °C. Next, SYBR® dye (500 μL) was added to the dispersion and was allowed to react with the free DNA chains for 20 min.

2.4 Calculation of the dextran thickness onto the MNPs surface

The thickness of the polymer layer onto the MNPs surface was calculated from the TGA analysis using equation: $h_{DX} = \frac{V_{DX,tot}}{S_{MNPs,tot}}$ (eq. 1), with $V_{DX,tot} = \frac{m_{DX}}{\rho_{DX}}$ and $S_{MNPs,tot} = S_{MNP}\ x\ N_{MNPs/gr}$, where, m_{DX} is the mass of the DX calculated from TGA, the density of the polymer $\rho_{DX} = 1\ g/mL$, $S_{MNPs,tot}$ is the total surface of the MNPs and S_{MNP} is the surface of a single MNP, and $N_{MNPs/gr}$ is the number of MNPs per gram.

2.5 Characterization Techniques

ATR–FTIR spectra were recorded on a Thermo Scientific Nicolet 6700 spectrometer. The freeze-dried samples (~5 mg) were placed in contact with the ATR crystal and the spectra recorded in the 400 – 4000 cm^{-1} wavelength range at a resolution of 2 cm^{-1} and number of scans 64. The DX-coated NPs were characterized by thermogravimetric analysis (TGA) using a Perkin Elmer Diamond TG/DTA system. Measurements were carried out in the temperature range between 30–550 °C, at a heating rate of 10 °C/min, under a nitrogen atmosphere. The weight of the samples used for each TGA measurement was 10 mg and all samples were measured once. The morphology of the bare and the DX-coated MNPs was determined by transmission electron microscopy (TEM), using a JEOL JEM-2100 microscope. The TEM samples were prepared by the deposition of one drop (10 μL) of an aqueous dispersion (0.01 mg mL^{-1}) of the NPs, onto a carbon coated Cu grid and was allowed to dry overnight at room temperature. The fluorescence intensity of the SYBR® dye at 520 nm, after its interaction with the free DNA chains in solution, was recorded on a Thermo Electron Varioscan fluorescence spectrometer upon excitation at 480 nm. The samples (300 μL of each sample) were transferred in a 96 well black bottom plate and were measured in triplicates.

2.6 DX-MNPs and DNA-DX-MNPs stability testing by TGA

The DX-MNPs (0.05 mg mL^{-1}) were treated with aqueous NaCl solutions at salt concentrations 0.01, 0.1 and 1 M for 24 h. Then, the DX-MNPs were purified to remove the salt via 5 centrifugation/redispersion cycles. For each purification cycle, the DX-MNPs were dispersed in 10 mL water and were sonicated in an ultrasound bath for 1-2 min prior to centrifugation. Right after, the samples were freeze dried for 48h and were characterized by TGA. A similar procedure was followed for the DNA-DX-MNPs.

3. Theory and Calculations

3.1 Systems. The systems studied in simulations are described in Table 1. Three systems were considered: DX-coated MNPs in water, an aqueous solution of DNA with DX-coated MNPs and a control system comprising the uncoated MNPs and DNA in water. The DX chains consisted of 10 hydroxylated monomer repeat units, whereas a 24-nucleotide sequence of a double-stranded DNA was used (Calf Thymus DNA (PDB ID 121D) $(CGCAAATTTGCG)_2$, with an adenine-thymine to guanine-cytosine pair ratio of 0.5, comparable to the experimentally studied base pair ratio).[41] At physiological pH conditions and at ionic strength levels similar to those considered in the present study, the hydroxylated DX molecules are expected to remain non-ionized, [42-44] while DNA nucleotides are expected to be negatively charged. [2, 45] The chemical structure of dextran is shown in Figure SI-1.

Table 1: Characteristics of the simulation systems

Systems	DX-coated MNPs	DX-coated MNPs and DNA	MNPs and DNA (Control)
Number of DNA chains (End-to-end distance)	-	10 (3.76 nm)	10 (3.66 nm)
Number of DX chains	96	96	-
Fe_3O_4 Surface	2 (mirror images) 11.74 x 11.74 nm^2	2 (mirror images) 11.74 x 11.74 nm^2	2 (mirror images) 11.74 x 11.74 nm^2

Number of Water molecules	72058	75698	73435	73194	79638
Number of Ions - Ionic Strength (M)	200 - 0.06	500 - 0.15	219 - 0.06	419 - 0.13	419 - 0.13

Initial configurations of two mirror periodic magnetic surfaces of Fe_3O_4 were set up, in a simulation box of 11.74 x 11.74 x 20 nm^3. Details for the unit cell of Fe_3O_4 are given in reference [46]. The two magnetic surfaces were kept fixed in space in all the examined models. The overall surface charge was taken to be equal to zero. Although a measurement of the ζ-potential in the "as-received" bare MNPs was -20 mV, yielding a net charge per unit surface area of -0.127 $|e|/(nm)^2$, other measurements in magnetite MNPs following a well-controlled synthetic protocol resulted in a measurement of ζ-potential of -8mV, indicating an even lower surface charge.[47] Due to this rather low surface charge, and the fact that the point of zero charge for magnetite is reported to be within the range of physiological pH conditions[48-50] an overall neutral magnetite surface was considered as an appropriate model for the conditions studied in the present work. Partial charges of the iron and the oxygen atoms were assigned according to reference [51], corresponding to a magnetite surface in contact with water. The DX molecules initially distributed in the simulation box formed an interfacial layer of physically absorbed chains on both surfaces after a few tens of ns of Molecular Dynamics (MD) steps. This setup was used for the construction of an aqueous solution of double-stranded DNA molecules, which were uniformly distributed in the simulation box. An appropriate amount of Na^+ and Cl^- ions was added to maintain the overall electrical neutrality of the systems, and to create solutions of different ionic strengths. This final configuration served as a starting point for the simulation runs.

Although the simulation model invokes a planar magnetic surface, while the experimental systems contain spherical magnetic nanoparticles, the comparison is reasonable at the length scales of the investigated properties. The size ratio of the radius of the nanoparticle over the linear size of the DNA chains (i.e., the end-to-end distance, R_{ee} (Table 1)) is very large, indicating that for the dimensions of the DNA chain the shape of the surface can be considered as flat without loss of generality.

3.2 Methods. All-atom Molecular Dynamics simulations were performed using the GROMACS package.[52] Both the DNA and polysaccharide molecules were modeled through the

CHARMM36 all atom force field.[53-55] Water molecules were described explicitly with the TIP3P model.[56] The particle-mesh Ewald (PME) algorithm with cutoff distance of 1 nm was used for the evaluation of the electrostatic interactions, whereas non-bonded interactions were parameterized through a spherically truncated *6-12* Lennard-Jones potential, with cutoff distance of 1 nm and standard Lorentz-Berthelot mixing rules. The time step for the integration of the equations of motion was 0.5 fs. Since the total volume of the simulation box was bounded by the spatially fixed magnetic surfaces, the simulations were performed using the isochoric-isothermal (NVT) ensemble. The temperature was kept constant at 300 K using the velocity rescaling thermostat.[57] Periodic boundary conditions were applied in all three directions. Simulation runs of 130 ns were performed, whereas the last 50 ns of the trajectory, where the systems had reached a steady conformational state, were used for the statistical analysis at equilibrium conditions.

4. Results

4.1 DX-Coated Nanoparticles

4.1.1 Simulations. Since the coating enhances the functionality and protects the NPs from agglomeration, its stability on the nanoparticle surface is highly desirable. In many biological processes the ionic strength plays an important role on the surface interactions and varies between I = [0.13 – 0.16] M in living organisms.[58] The stability of the physically adsorbed polysaccharide layer onto the magnetic surface was examined under two different ionic strength conditions. At a low value of I = 0.06 M, which represents the case of ultrapure water, and at values of I=0.13 M and 0.15 M, which are commensurate to the physiological ionic strength levels in the human body. Figure 1b portrays a snapshot of the system comprising the magnetic surfaces with the adsorbed DX layer in an aqueous environment. For both values of ionic strength examined, no sign of DX desorption from the magnetite surface was observed in the examined simulation window. The density profiles at three different time spans (i.e., 4, 8, 12 ns), after the commencement of the simulations, together with the average profile corresponding to the entire simulation window, are shown in Figure 1a for I = 0.15 M. Evidently, the profiles overlap, signifying that as soon as the interfacial layer was formed, it remained stable throughout the simulation. For the amount of DX considered, the polysaccharide layer reached a thickness of approximately 2 nm, as indicated in Figure 1a (the black vertical lines mark the boundaries of the magnetic surface with a thickness of

about 1 nm). Practically identical density profiles were observed for both systems at the different ionic strengths examined.

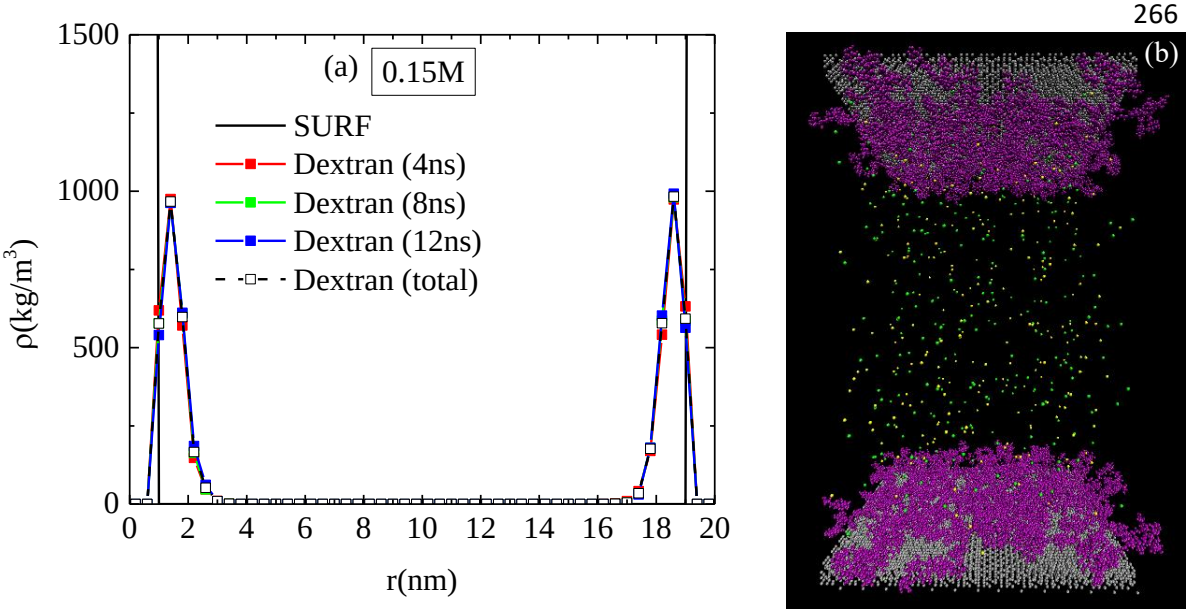

Figure 1. a) Average density profiles of DX at I = 0.15 M, corresponding to three different time periods of the simulation. The vertical lines indicate the boundaries of the magnetite surface; b) Characteristic snapshot of a model system of DX-coated magnetic surfaces after the formation of the DX layer; the yellow and green dots represent the Na^+ and Cl^- ions, respectively. DX is shown in purple. Water molecules are omitted for clarity.

The similarity between the density profiles at different time periods from the commencement of the run (starting from the non-adsorbed state) shows that the kinetics of the DX adsorption on the magnetic surface is a fast process with a timescale of the order of few ns. Since the DX molecules are physically adsorbed, instead of being chemically attached on the surface, the interfacial layer is not immobile. Lateral motion along the surface was detected, while the motion normal to the surface was very limited. The mean square displacement (MSD) in the directions parallel and perpendicular to the surface, quantifies the dynamics of the polysaccharide molecules. MSDs for the center of mass of the polymeric chains are presented in Figures 2a and 2b for the motion perpendicular and parallel to the surface, respectively, at both ionic strength values. MSDs in the

xy-plane are more than one order of magnitude higher than the ones along the z-axis (i.e., perpendicular to the surface). Although the DX molecules move faster laterally along the plane, their motion is in general limited, due to their adsorption onto the inorganic surface. A small difference in MSD was observed between the lower and the higher values of the ionic strength, rendering the diffusive motion of DX faster in the former case, in both directions. This indicates that at higher ionic strength conditions (i.e., within the range of I values corresponding to the physiological conditions) the DX layer is adsorbed more firmly on the magnetic surface.

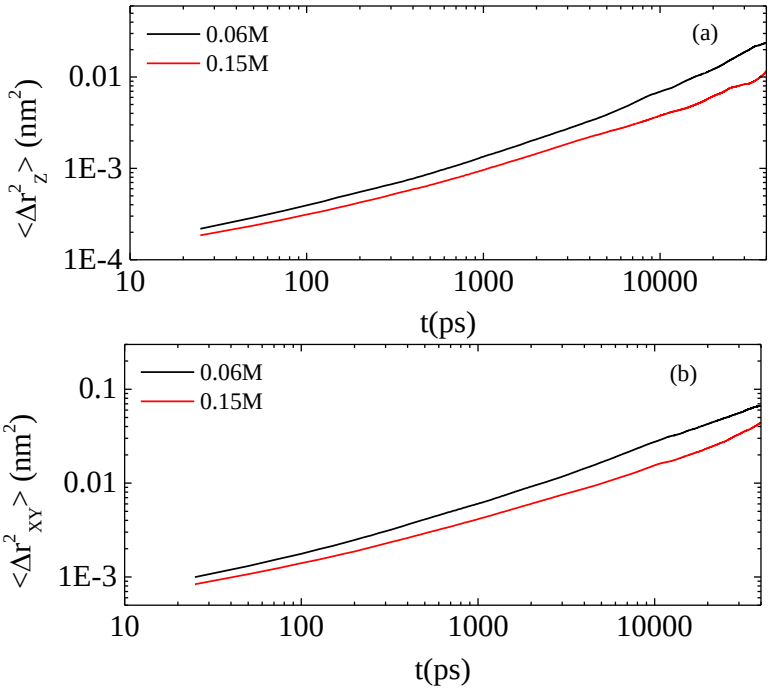

Figure 2. Mean squared displacement as a function of simulation time for the center of mass of the DX chains in a direction (a) perpendicular and (b) parallel to the magnetic surface at two different ionic strength values.

The structural stability of the adsorbed DX layer is a result of the energetic interactions between the magnetic surface and the polysaccharide molecules. The origin of the energetic affinity between the coating and the surface was determined by separately examining the two main contributions, that is the electrostatic and the Van der Waals interactions. Figure SI-2, in the Supporting Material, shows that both interactions favor attraction, with the Coulombic forces contributing the most. A small difference in the attractive energy between I = 0.06 M and I = 0.15

M, in favor of the latter, is consistent with the slower motion of the DX molecules at the higher I value, as noted in Figure 2.

4.1.2 Experiments. The surface of the MNPs was functionalized with the hydrophilic polysaccharide via an ex-situ preparation method, during which the MNPs were mixed with the DX solution at a 1:5 MNPs:DX mass ratio. TEM images of the uncoated and the DX-coated MNPs revealed that the presence of the DX layer on the MNPs surface, decreased the tendency of the MNPs to form large agglomerates compared to the bare MNPs (Figure SI-3). The average diameter of the MNPs was found 35 ± 17 nm (Figure SI-3c). Figure 3a, shows the ATR-FTIR spectra of the uncoated MNPs, DX and the DX-coated MNPs. The appearance of the stretching vibration mode of Fe-O at 544 cm^{-1}, along with the vibration bands at 1012 cm^{-1} and 1355 cm^{-1} corresponding to the C-O bonds of the polymer, and the peaks at 1642, 2900 and 3300 cm^{-1} attributed to the -CH and -OH vibrations of DX, confirmed the successful coating of the MNPs with the polymer chains. The amount of DX deposited onto the surface of the MNPs was found to be approximately 9 wt% by TGA (Figure 3b, green line). The thickness of the DX layer deposited onto the MNPs surface was calculated from TGA using eq. 1 and was found to be ~5.8 nm, which is of the same order of magnitude as the model system.

To examine the effect of the ionic strength on the stability of the polymer layer on the MNP surface, the DX-coated MNPs were incubated in aqueous NaCl solutions at various salt concentrations ranging from 0.01 M to 1 M for 24 h. The nanoparticle suspension was thoroughly purified through several centrifugation/redispersion cycles to remove NaCl and the potentially detached polymer chains. As shown in Figure 3b, all samples exhibited similar weight loss around 9 wt% and, importantly, insignificant (~1 wt%) detachment of the DX chains from the MNPs was observed, denoting the stability of the coating on the MNP surface at the different ionic strength conditions. These experimental results are in good agreement with the findings of the simulation study described above, concerning both the stability of the coating layer and the negligible effect of the ionic strength of the solution at the examined levels, regarding the presence of the DX-layer onto the magnetic surface.

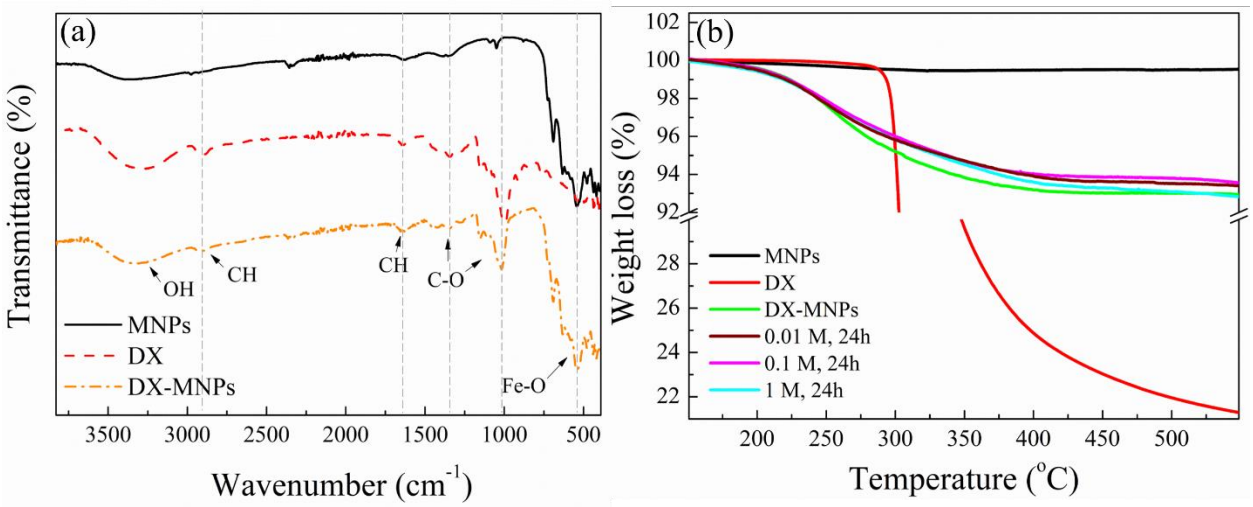

Figure 3: (a) ATR-FIR spectra of the MNPs, DX and the DX-coated MNPs, (b) TGA curves for the MNPs, DX and the DX-coated MNPs before and after incubation in aqueous NaCl solutions of 0.01 M, 0.1 M and 1 M for 24 h.

4.2 DNA – Magnetic Nanoparticle Systems

4.2.1 Simulations

4.2.1.1 Effect of Ionic Strength

After confirming the stability of the interfacial DX layer, DNA molecules were introduced in the aqueous solution, by uniformly distributing them in the simulation box between the two magnetic surfaces. The two catoptric surfaces were placed far from each other to avoid any confinement effects for the DNA molecules (the separation between the two magnetic surfaces, Lz = 20 nm, was significantly larger than the DNA end-to-end distance). Soon after their introduction, a tendency of the DNA molecules to approach the surface was observed. This trend resulted in the physical adsorption of DNA on the surfaces after approximately 80 ns, as discussed in more detail below. Density profiles for all the components of the system at I = 0.13 M, calculated from the part of the trajectory in which kinetic effects have subsided, are presented in Figure 4a.

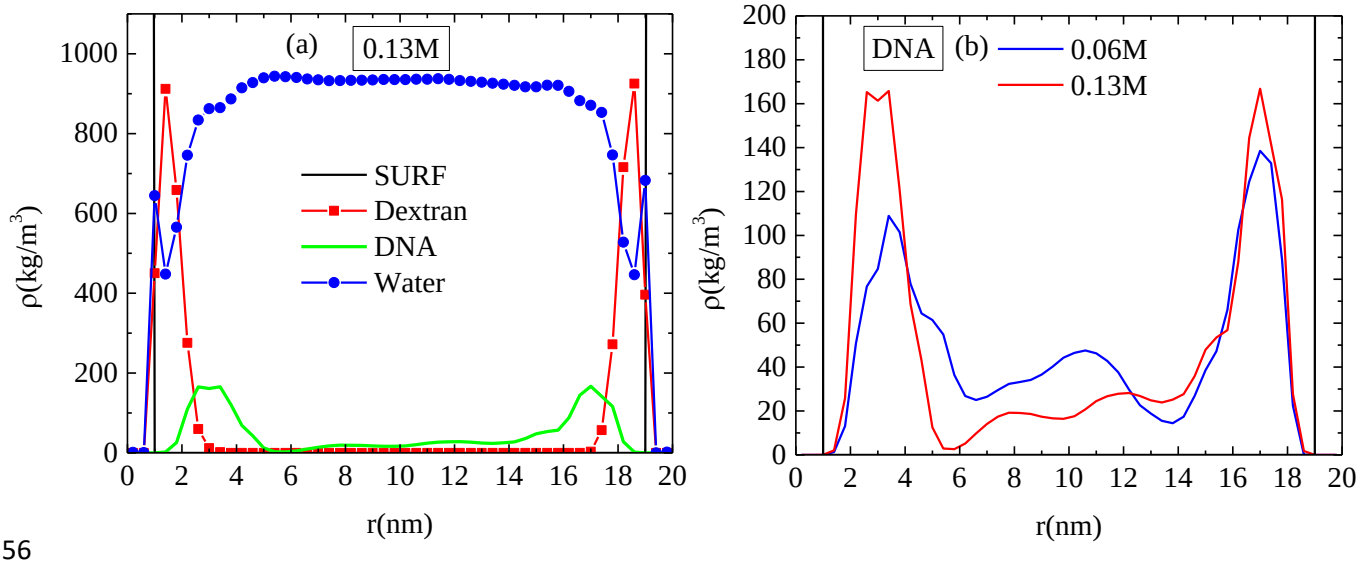

Figure 4. (a) Density profiles of all the components of the system along the z-direction of the simulation box (i.e., perpendicular to the surface) at I = 0.13 M. (b) Density profiles of DNA along the z-direction for two systems at I = 0.06 M and I = 0.13 M. Vertical lines denote the boundaries of the magnetic surfaces.

Two practically symmetric layers of DNA molecules were formed, partially overlapping with the DX coating profiles. The DNA density profiles assumed a much lower density, due to the very low concentration of DNA in the simulated system, in line with the corresponding experiments, discussed below. A minor degree of penetration into the DX coating was observed for DNA, indicating that part of the DNA came closer to the magnetic surface, but did not adsorb onto it. The bulk region in the middle of the simulation box was almost entirely occupied by water, although a small amount of water was also detected in the DX layer. Comparison of the DNA density profiles in the two systems at different ionic strengths (0.06 M and 0.13 M), showed a somewhat higher DNA density at the interface for I = 0.13 M, as indicated by the corresponding higher peak intensities in Figure 4b. The density profiles were not fully symmetric with respect to the specular magnetic surfaces due to the low concentration of DNA. Slightly more unbound DNA was found in the middle of the simulation box at the lower I value.

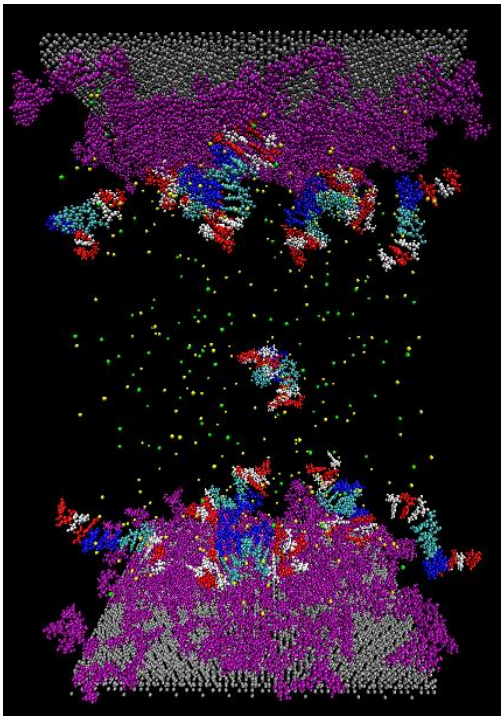

Figure 5. Snapshot of a model system with the 12-nucleotide DNA molecules inserted into the aqueous environment between the two DX-coated magnetic surfaces at I = 0.13 M, at a time when physical adsorption of DNA onto the DX layers has been achieved. DX is portrayed in purple, DNA is shown as colored (blue, red, white) strands, while the yellow and green dots represent the Na^+ and Cl^- ions, respectively. Water atoms are omitted for clarity.

A typical snapshot of the system at I = 0.13 M at a timescale where the DNA adsorption onto the DX layer has been already realized, is shown in Figure 5, in which the majority of the DNA strands are observed to lay on the DX coating, while a small amount of DNA remains unbound. Beyond 80 ns, when physical adsorption has progressed, spontaneous DNA detachment and re-attachment events are rarely observed during the simulation, resulting in the average DNA density profile shown in Figure 4. Furthermore, the average dimensions of the DNA strands do not seem to be affected by their interaction with the DX layer. This behavior is demonstrated in Figure SI-4 where the end-to-end distance and the radius of gyration of the DNA molecules are shown as a function of time during the entire simulation.

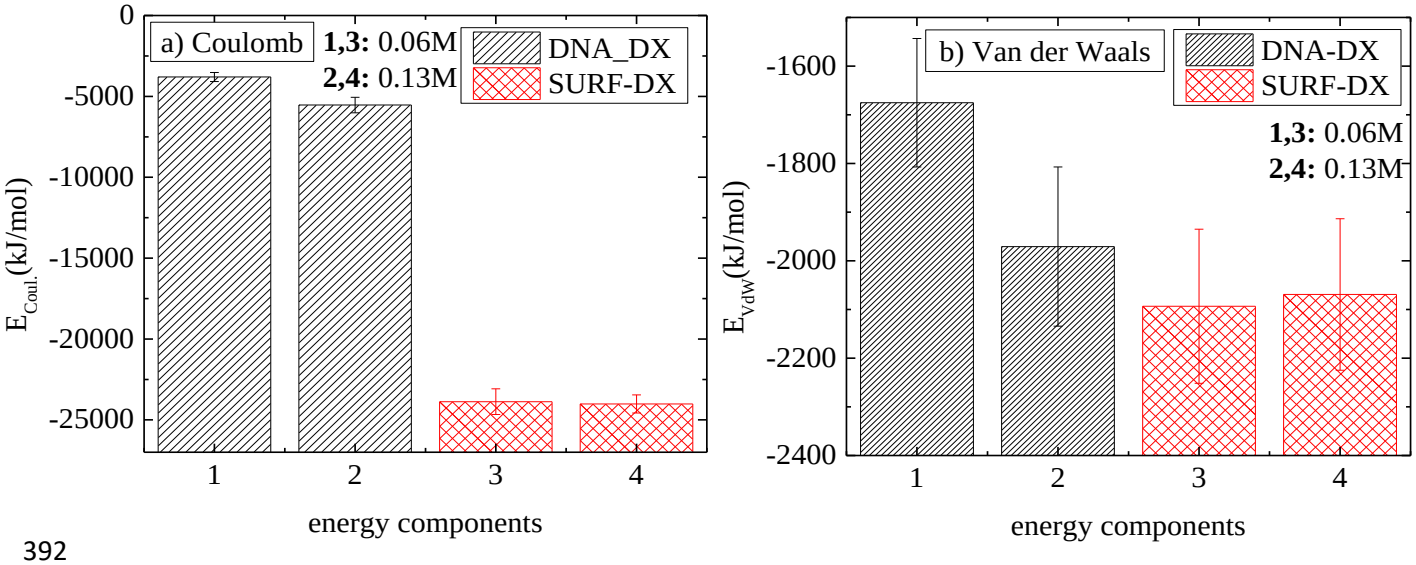

Figure 6. Average values of energetic components over the equilibrated part of the trajectory for the systems comprising the DNA strands and DX-coated nanoparticles at I = 0.06 M and I = 0.13 M. (a) Coulomb interaction energies between DX and the magnetic surface and between DX and DNA, (b) Van der Waals energies between DX and the magnetic surface and between DX and DNA.

Differences in the DNA binding strength for the systems at different ionic strengths can be mapped by examining the interactions involved in the adsorption process. Average values of the relevant energetic components have been calculated over the last 50 ns of the trajectory, where the adsorption process has been completed. Figure 6a displays the energetic contribution arising from the electrostatic interactions between the magnetic surface and the DX chains and between the DX layer and the DNA strands at both ionic strengths. The DNA-DX electrostatic interactions became moderately more attractive at the higher ionic strength, whereas no such effect was detected for the interactions of the magnetic surface-DX pair. Because of the intervention of the DX layer and the electrostatic screening provided by the counterions, the forces between the DNA strands and the magnetic surface are very weak, as will be discussed in Section 4.2.1.2 below. Comparing the energetic contribution arising from the van der Waals interactions between the magnetic surface and the DX chains and between the DX layer and the DNA strands (Figure 6b), an enhanced attraction between the DX and DNA chains on average, was observed at the higher ionic strength (I = 0.13 M), while the magnetic surface-DX interactions were similar and strongly attractive at both I-values. The latter indicates that the principal driving force for the formation of a stable DX layer near the surface

is the electrostatic interactions between the partial charges of the magnetite surface and those of the DX molecule. Apart from the strength of the Coulombic and the Van der Waals interactions between the different components at the final state, information for the kinetics of the binding process is provided in Figure SI-5, where the various energetic contributions are presented as a function of time during the simulation.

The time dependence of the energetic components seems to change slope at a timescale close to 80 ns, when the relevant energies approach values very close to their equilibrium levels. Statistical analysis of the equilibrium properties that will be discussed onwards, is based on the part of the trajectory beyond this timescale. Furthermore, as it was expected, the total potential energy of the system decreased in its equilibrium state compared to the starting point of the simulation runs (initial configuration). In Figure SI-6 in the Supporting Material, the potential energy of the system in the initial configuration is juxtaposed with the potential energy in the final configuration for both I-values. The difference between the initial and the final states is more pronounced for the higher ionic strength system, which is consistent with a stronger driving force towards equilibrium. The system rests at a state with stronger attractive interactions when the I-value is higher, indicating a higher energetic stability, in line with the trend exhibited by the partial energetic components in Figure 6.

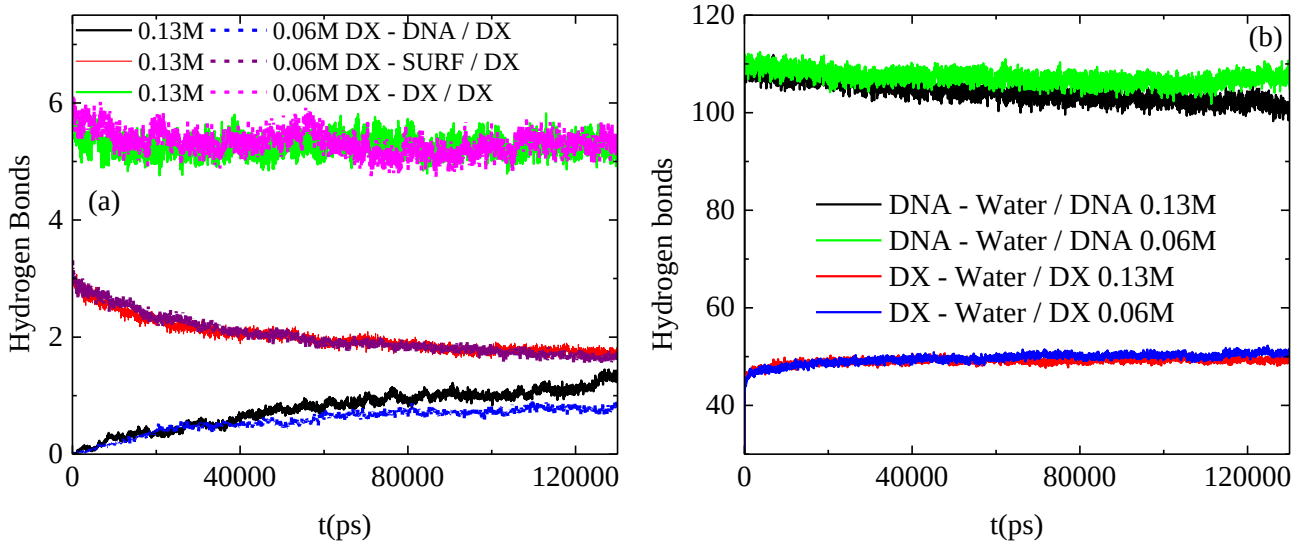

Figure 7. Average number of hydrogen bonds as a function of time from the commencement of the simulation at I = 0.06 M and I = 0.13 M formed between (a) DX-DNA (black 0.13 M; blue 0.06 M), DX-DX (green 0.13 M; magenta 0.06 M) and DX-magnetic surface (red 0.13 M; purple

0.06M); solid lines correspond to I = 0.13 M and dash-dot lines to I = 0.06M; (b) DX-water (red 0.13 M; blue 0.06 M) and DNA-water (black 0.13 M; green 0.06 M). All curves except for the DNA-water pair, are normalized with the number of DX chains (denoted by the "DX" notation). The latter pair is normalized with the number of DNA molecules.

An additional mechanism relevant to the association between the components of the system, is hydrogen bonding (HB). While the HB interaction is also of electrostatic nature, it deserves special attention because it also encompasses the specific relative arrangement of the hydrogen donor and acceptor pairs necessary for its formation, which can contribute to the structural stability of the formed complexes. Hydrogen bonds can be formed between all pairs of molecules present in the systems, since they bear hydrogen-bonding donors and acceptors.[59-60] It has previously been demonstrated that polysaccharides such as DX can form hydrogen bonds with the oxygen atoms of the magnetite surface.[61] In our case the surface density of the oxygen atoms are 11 sites/nm^2. Here the definition of a hydrogen bond is based on geometric criteria involving the distance (r) between a donor (D) and an acceptor (A) ($r \leq 0.35$ nm) and the angle formed by the hydrogen (H), the donor and the acceptor ($\alpha_{HDA} \leq 30^o$). The evolution of the number of hydrogen bonds with time is presented in Figure 7 for both the I-values examined. In Figure 7a solid lines correspond to I = 0.13 M, while dash-dot lines to I = 0.06 M. The values presented are normalized to the number of DX molecules. Evidently, the DX molecules form a larger number of hydrogen bonds per chain with the other polysaccharide molecules, compared to the hydrogen bonds formed between the DX and DNA chains or the DX and the magnetic surface, at both I-values. This DX-DX interaction leads to a stronger self-association between the DX molecules and thus to the formation of a firmer coating layer, while the formation of hydrogen bonds between the magnetic surface and the DX molecules even at these rather lower levels enhances the DX-surface cohesion. The relatively low number of hydrogen bonds between DX and DNA per DX molecule, indicates that hydrogen bonding is not the main driving force for the DNA/DX association, but rather serves as an auxiliary factor. The slightly higher number of hydrogen bonds formed between DNA and DX at higher ionic strength (I = 0.13 M), favors the formation of more stable DNA/DX complexes at these conditions.

The number of hydrogen bonds formed between the different components and the water molecules is presented in Figure 7b. Hydrogen bonding between the DX chains and water was hardly affected by the ionic strength at the range examined in this work. On the other hand, DNA strands formed

a somewhat higher number of hydrogen bonds with water at I = 0.06 M compared to that at I = 0.13 M. This is consistent with the increased hydrogen bonding level between DNA and DX at I = 0.13 M, implying that at this ionic strength fewer DNA hydrogen-bonding sites remain available for the water molecules to associate with. In this context, the energy differences between the DNA and DX interactions corresponding to the two ionic strengths as depicted in Figure 6, can be rationalized; they may originate from the higher availability of DNA hydrogen-capable-sites due to the formation of a lower number of hydrogen bonds with water at higher ionic strengths. The higher availability of DNA sites for hydrogen bonding with DX, allows for the enhancement of their interaction upon increase of the ionic strength.

The abovementioned interactions are expected to affect the motion of the adsorbed molecules on the magnetic surface as well. As discussed above, a rather limited motion of the interfacial DX layer in the DNA-free systems was observed, mainly in the direction parallel to the surface. Herein we explore the motion of the DNA strands on top of the DX layer. The mean squared displacement of the center of mass of the DNA molecules in the direction parallel to the surface and perpendicular to it, is presented in Figure 8a together with the total (3D) MSD at I = 0.13 M. Figure 8b provides for comparison the same information for the DX molecules at I = 0.13 M in the presence of DNA. The MSDs were calculated over the late part of the trajectory (i.e., the last 50 ns), when binding kinetics were practically completed. Notably, the motion of DNA was found much faster compared to that of DX (i.e., more than 2 orders of magnitude faster) both in the parallel and the perpendicular direction with respect to the surface. This is consistent with the much lower energetic affinity between DX and DNA compared to that between DX and the magnetic surface, as noted earlier (see Figure 6). The xy-component of the DNA MSD (parallel to the surface) is about 5 times faster than its z counterpart (perpendicular to the surface). It should be noted that the z-component encompasses also the displacement due to rare spontaneous events, during which the DNA molecules detach from the surface.

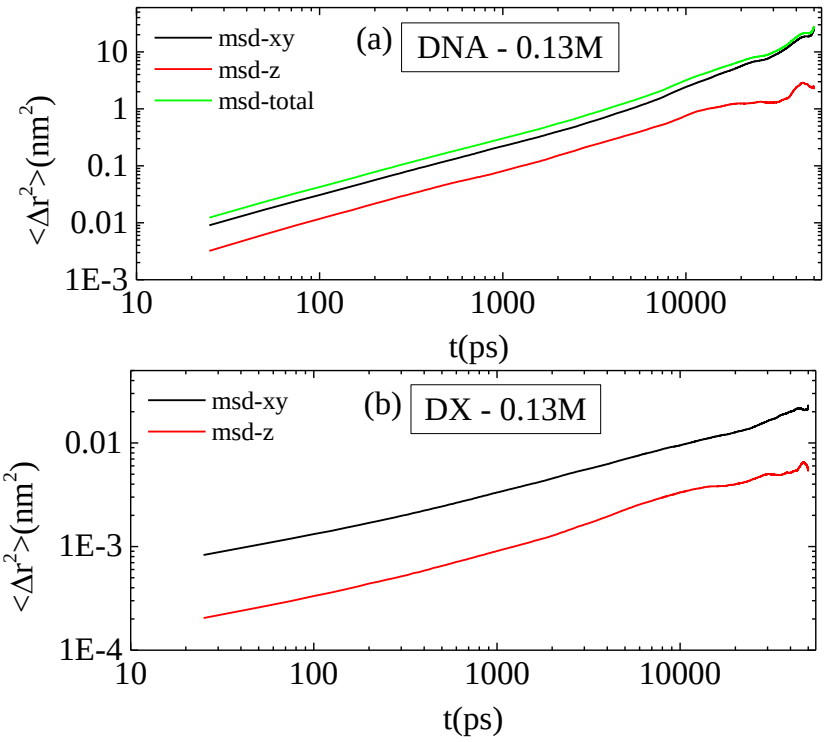

Figure 8. Mean squared displacement as a function of time, over the part of the trajectory where no binding kinetics are involved, for the center of mass of (a) the DNA strands and (b) the DX chains at I = 0.13 M.

4.2.1.2 Effect of the Coating

In order to highlight the effect of the coating and its impact on the DNA binding process, a system comprising uncoated magnetic surfaces and DNA at I = 0.13 M was examined as a control case. The properties of this system were compared to those found for the DX-coated magnetic surfaces with DNA. The snapshot in Figure 9, after a 130 ns simulation run, indicates a rather poor adsorption of the DNA strands on the uncoated magnetic surfaces. This picture is consistent with a rather frequent detachment events of the DNA molecules from the magnetic surface, leading to an overall less stable binding of DNA.

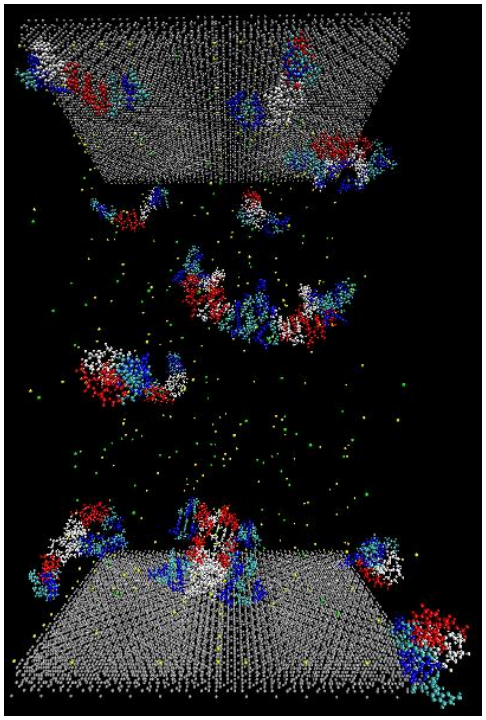

Figure 9. A typical long-time snapshot of a model system comprising DNA strands immersed in an aqueous environment between two uncoated magnetic surfaces at I = 0.13 M. The DNA strands are represented as colored (blue, red, white) molecules, whereas the yellow and green dots correspond to the Na^+ and Cl^- ions, respectively. Water molecules are omitted for clarity.

From the energetic point of view, the above findings are supported by the overall much weaker interactions involved in the association of DNA with the surface, as illustrated in Figure 10. The different energetic contributions associated with the interactions between the DNA strands and the magnetic surfaces are juxtaposed in Figures 10a and 10b for the systems with the uncoated and DX-coated surfaces, respectively. In both cases, a small attraction originating from the dispersion Van der Waals forces between the DNA strands and the magnetic surfaces is observed, while a weak Coulombic repulsion is also evident with the uncoated surface. In addition, practically no hydrogen bonding interactions were detected between the DNA strands and the magnetic surfaces. The presence of a few DNA strands near the magnetic surface (Figure 9), may originate from the presence of a layer of sodium counterions located near the magnetic surface, which exerts Coulombic attractions to the DNA molecules.

The density profiles of the ions in the systems comprising the DNA strands in the presence of the coated and uncoated magnetic surfaces at I = 0.13 M are presented in Figure SI-7. Although in both cases an excess of Na^+ ions was found near the surface,[37, 59] their localization was significantly stronger near the uncoated magnetic surface causing the partial condensation of DNA. A small fraction of Cl^- ions was also found close to the uncoated magnetic surfaces, whereas most of the Cl^- ions were uniformly distributed within the aqueous phase when the surfaces were coated with DX.

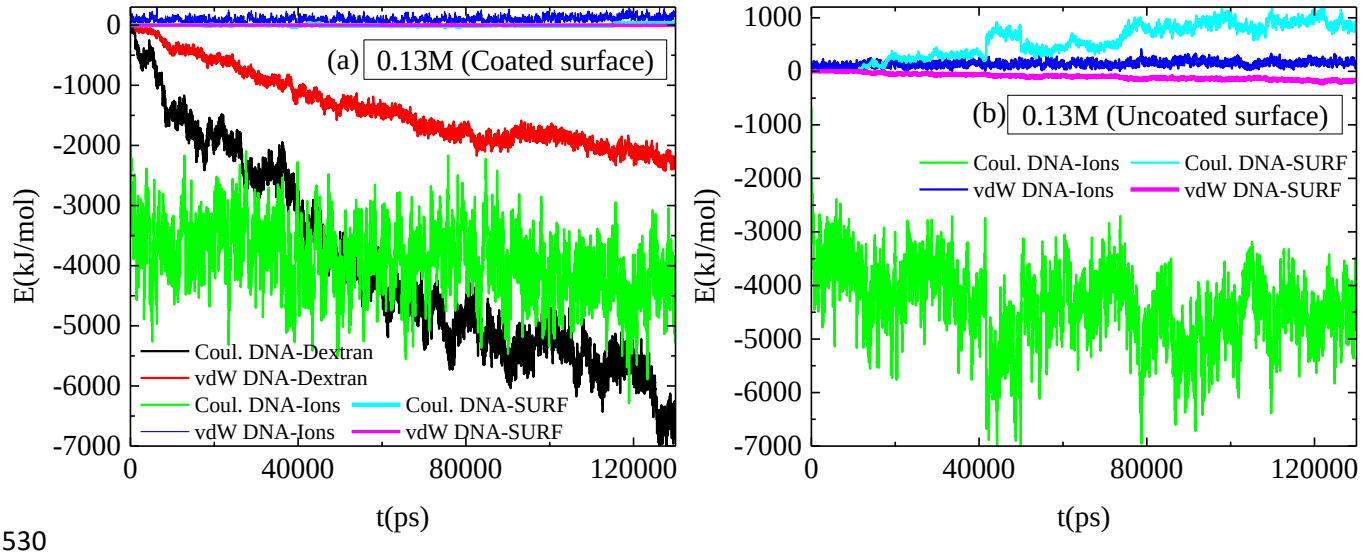

Figure 10. Energy components as a function of time for (a) the system comprising DNA and DX-coated magnetic surfaces and (b) the corresponding system with DNA and the uncoated magnetic surfaces (control), at I = 0.13 M.

Figures 11a and 11b present the MSD of the DNA strands' center of mass in the directions parallel and perpendicular to the surface, respectively, at I = 0.13 M. Comparison of the MSDs of the DNA molecules in the two systems, with the DX-coated and the uncoated surfaces, showed that DNA displacement was realized faster in the latter system, in both, the xy- and z- directions. Faster motion near the surface implies a weaker localization and thus, a rather unstable association of DNA with the surface, in line with the discussion above regarding the energetics of this system. Since the main driving force attracting the DNA strands near the uncoated magnetic surfaces appears to be the formation of a Na^+ ion layer, this is expected to be rather sensitive to variations in the ionic strength

of the system and therefore, would lead to unstable DNA/MNPs complexes upon local variations of the ion concentration during the delivery process within the human body.

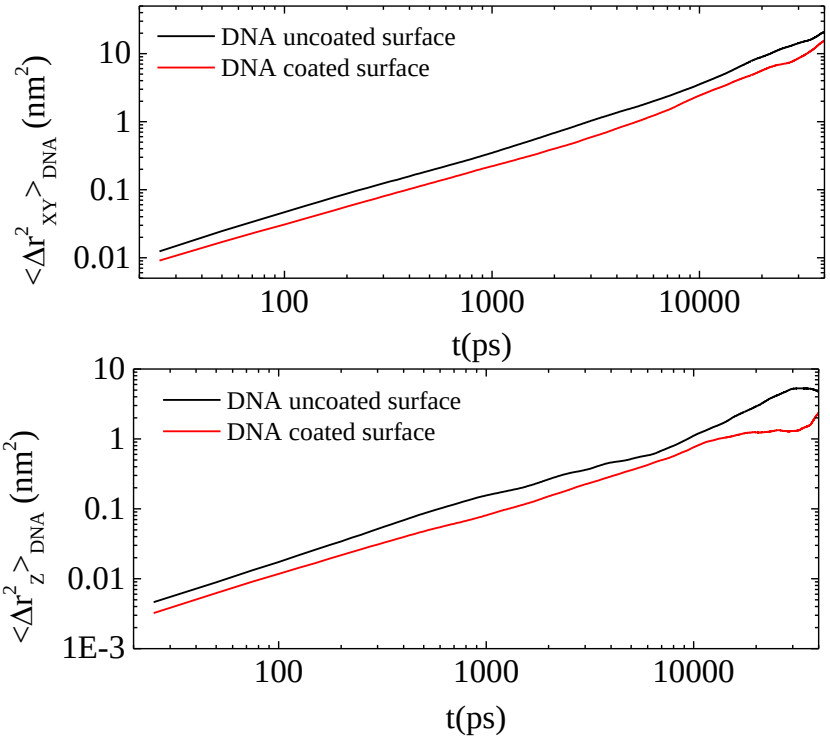

Figure 11. Mean squared displacement as a function of time, over the part of the trajectory in which the adsorption kinetics were completed, for the center of mass of the DNA strands in the systems comprising DX-coated (red solid line) and uncoated (black dashed line) magnetic surfaces at I = 0.13 M, for the (a) xy-component and (b) z-component.

4.2.2 Experiments

To check the predictions made by the simulated models and to further elaborate on the results obtained from the computational study, we have also carried out a series of experiments, to examine the effect of ionic strength on the interactions/binding of the DNA strands onto DX-coated MNPs and the stability of the polymer layer in the presence of DNA. For this purpose, DNA from Calf Thymus, as a model gene sequence, was used. DX-coated MNPs and DX-coated MNPs complexed with DNA were dispersed in a 0.1 M NaCl aqueous solution at pH 7.4 for 24 h. The calculation of the weight loss from TGA analysis is presented in Table SI-1, where the DX content of each sample is presented. The respective DX weight loss is summarized in Table 2.

Fluorescence probe is not included in this solution. As already mentioned above to secure the validity of the TGA measurements, all samples were measured after thorough purification and removal of the salt. It is expected that the polymer chains which have been detached during the treatment under the different ionic strength conditions will be removed after the purification process. Consequently, the TGA analysis was used to calculate the amount of the remaining, attached dextran chains, meaning those that have not been affected by the solution conditions or the presence of the DNA. As seen in Figure 12 and Table 2, the DX-coated MNPs exhibited almost the same decrease in the weight loss in the presence and absence of salt and the remaining ~9 wt% of the DX content thus constitutes the coating layer. This observation indicates that almost the entire polymer layer remains attached to the magnetic surface during the treatment, indicating the stability of the polymer layer at the examined ionic strength conditions. This experimental result is aligned with the findings of the simulation study.

In addition, TGA measurements show that the presence of DNA affects to a small degree the thermal stability of the polysaccharide layer. Namely, the DX-coated MNPs complexed with DNA in the presence of salt (I = 0.1 M) exhibited a weight loss similar to the one observed in DX-coated MNPs, without DNA, resulting in the same (i.e., ~9 wt%) of DX content. On the contrary, in the absence of salt, the weight loss was smaller by about 33% with respect to that observed in the sample containing salt. This indicates that in the absence of salt the mass of the adsorbed layer was diminished by this amount, prompting thus a weaker interaction between the surface and the DX/DNA complex.

These results are signifying that the presence of the Na^+ and Cl^- ions induce a small enhancement of the favorable interactions between the adsorbed polymer layer, the DNA molecules and the magnetic surface, conferring stability to the overall DNA-DX-MNPs system. This observation is in qualitative agreement with simulation findings that showed a stable polysaccharide layer on the magnetic surface at I values in the range 0.06M – 0.15M and a small enhancement of the DX bonding on the magnetic surfaces upon increasing the ionic strength.

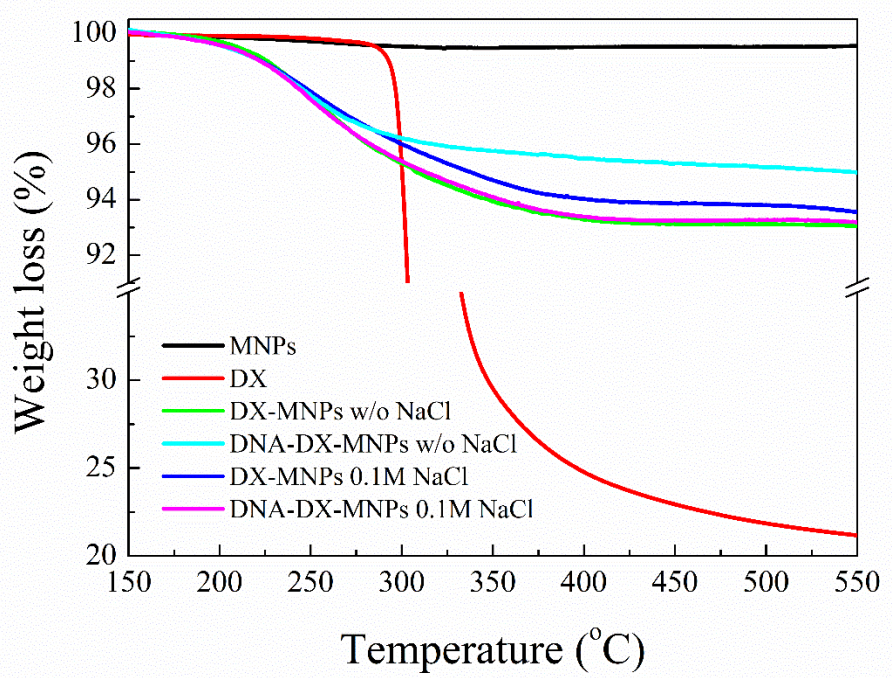

589

590 **Figure 12.** TGA curves of the DX-coated MNPs and the DX-coated MNPs complexed with DNA
591 after equilibration in aqueous solutions in the presence and absence of 0.1 M NaCl. The TGA curves
592 of the uncoated MNPs and DX are shown for comparison. The notation "w/o" denotes the absence
593 of salt. The confidence intervals for TGA measurements can be estimated to about 1% as the
594 measurement instrumental error.

595 **Table 2.** DX content of the DX-coated MNPs and DX-coated MNPs complexed with DNA in the
596 presence and absence of NaCl.

Sample	DX content (wt %) by TGA
DX-coated MNPs	**100**
DX-coated MNPs at 0.1 M NaCl	**87%**
DX-coated MNPs complexed with DNA	**67% (33% weight loss)**
DX-coated MNPs complexed with DNA at 0.1 M NaCl	**100**

597

598 The interactions of DNA with DX and the DX-coated MNPs was confirmed by fluorescence
599 spectroscopy. A model aggregation-induced-emission fluorescence probe, SYBR green I (SG),
600 was utilized to detect the binding of DNA with DX and the DX-coated MNPs. SG emits a very

601 weak fluorescence signal when found in free form in solution, while its emission is significantly
602 enhanced upon interaction with free double stranded DNA chains (dsDNA), due to its restricted
603 intramolecular motions. The interaction of SG with the complexed DNA strands is hindered
604 allowing the detection only of the free dsDNA (non-complexed). Following the fluorescence signal
605 of SG, it was found that 60% of the DNA strands were complexed with the DX-coated MNPs
606 (Figure 13, blue bar) in the absence of salt. The complexation capacity of the DX-coated MNPs
607 was significantly enhanced, leading to a negligible number of free DNA strands, in the addition of
608 0.05 M NaCl. This, according to the simulation results, can be attributed first to the presence of
609 the Na+ ions close to the magnetic surface within the DX coating layer (Figure 4a and SI-7), which
610 increases the attractive forces between the DX-coated MNPs and the negatively charged DNA
611 chains. Second, in the formation of hydrogen bonds between DNA strands and DX chains on the
612 surface of MNPs, which is enhanced upon increase of the ionic strength, as noted in the simulation
613 results (Figure 7a). A further increase in the salt concentration to 0.1 and 0.15 M imparted a small
614 but measurable decrease in the fluorescence intensity indicating a small enhancement in the
615 complexation capacity of DNA with the DX-coated MNPs. The results are in line with the
616 simulation findings, where a considerable amount of DNA is detected close to the DX-coated
617 MNPs at both I-values (Figure 4). It is also observed that DNA could not effectively complex with
618 free dextran in the absence of salt (Figure 13, red bar), while DX can complex 60% of the DNA
619 when increasing the salt concentration in the solution to 0.15 M, as illustrated in Figure 13 (dark
620 cyan bar). This is probably related to the ion condensation on the DNA chains which can modify
621 the electrostatic interactions with DX (see Figure SI-7). Although the DNA-DX system in the
622 absence of the magnetic surfaces was not simulated, and therefore, a direct comparison between
623 the experimental and simulation results is not possible in this case, the observed behavior is
624 consistent with that found for the simulated DNA-DX-MNPs model discussed above. Therefore,
625 the experimental results in qualitative agreement with the simulation study indicate that the DX-
626 coated MNPs at biologically relevant ionic strength levels contribute synergistically to the
627 effective complexation of the gene strands with the MNPs, rendering this system a good candidate
628 for clinical gene delivery trials.

629

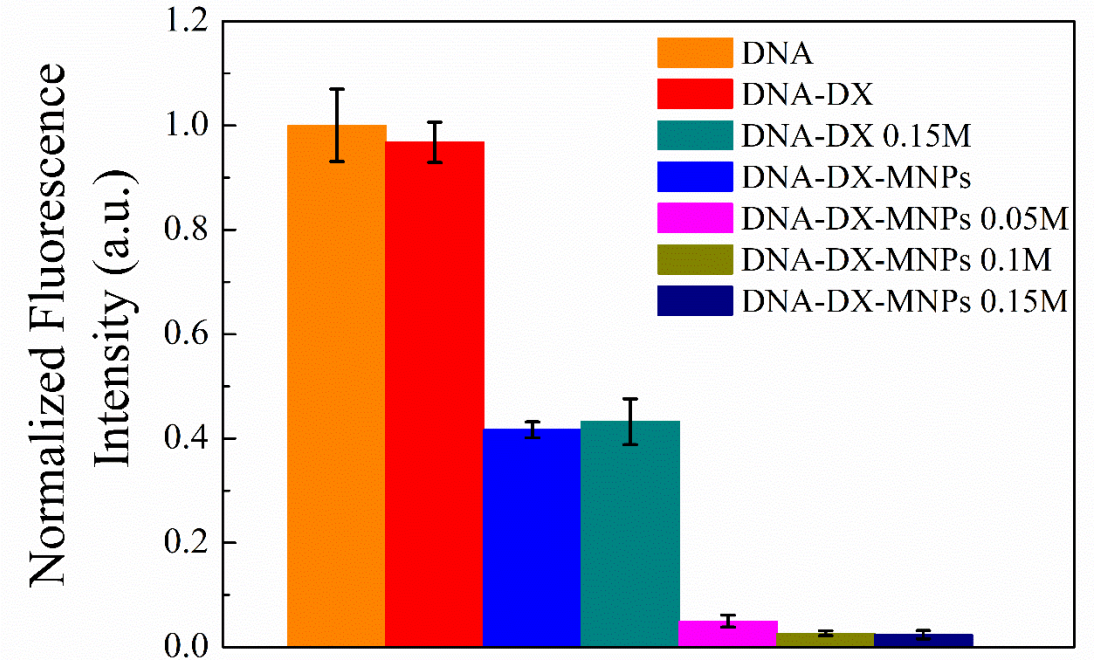

Figure 13. Normalized fluorescence intensity of SG in aqueous solutions of DNA, DNA with DX, and DX-coated MNPs complexed with DNA at various salt concentrations.

5. Discussion

The combination of all-atom Molecular Dynamics simulations with experimental data highlighted the significant role of the polymer coating on the surface of the MNPs in their DNA binding capacity.

The simulation studies revealed the formation of an interfacial layer of physically adsorbed DX molecules on the magnetic surfaces, which is stable and negligibly affected by the ionic strength at the examined levels. It was found that the dominant driving force for the physical adsorption of DX layer onto the magnetic surface is the Coulombic interactions between the surface and the polysaccharide molecules. The charge imbalance necessary for the Coulombic attraction between these two components (which were overall electrically neutral) was provided by the different degree of screening of their partial charges due to the uneven distribution of the salt ions. The Na^+ ions were preferentially located close to the magnetite surface, while the Cl^- ions were distributed almost evenly within the aqueous phase (see Figure SI-7). The uneven distribution of the salt ions in the aqueous phase and in the presence of the magnetite surface was found to be characteristic of the system since this was observed also in the absence of the DX-layer. The structural integrity of the DX layer was found to be augmented by the formation of hydrogen bonds between the DX

649 molecules. The degree of DX-DX hydrogen bonding was found to be insensitive to the ionic
650 strength at the examined levels.
651 The importance of the coating layer in the effective binding of DNA on the nanocarriers, was
652 highlighted through the simulation study of a control system, comprising bare magnetic surfaces,
653 at the same ionic strength conditions (I = 0.13 M). Weak Van der Waals interactions were the only
654 attractive forces between DNA and the magnetic surfaces, whereas part of the sodium ions formed
655 a thin layer near the magnetic surfaces, which exerted rather weak electrostatic attraction to the
656 DNA molecules. On the contrary, in the presence of the DX layer, successful complexation
657 between DNA and the MNPs was observed. This was accomplished through the interactions of
658 DNA with DX. The main driving force for the DNA-DX complexation was also found to be
659 Coulombic interactions. However, the DNA-DX interaction energy was weaker compared to that
660 of the surface-DX interaction.
661 Upon adsorption of DNA on the DX layer, no measurable changes in its conformational properties
662 could be observed, most probably due to its weaker adsorption but also due to the rather short
663 nucleotide sequence studied. The DNA-DX energetic stability was enhanced by an increase in the
664 ionic strength. This was found to be associated with the formation of a higher degree of hydrogen
665 bonding between the two types of molecules, which can be correlated to an analogous decrease of
666 hydrogen bonding between DNA and water, with the increase of the ionic strength. The
667 homogeneous dispersion of the Cl^- counterions within the aqueous phase contributes to the
668 disruption of the hydrogen bonding between water and DNA and thus to an enhanced availability
669 of hydrogen-bonding-capable sites, allowing DNA to form more hydrogen bonds with DX. At the
670 same time, due to the accumulation of the Na^+ counterions close to the magnetic surface where the
671 DX molecules were also located, a more effective screening of their overall negative charge was
672 realized, allowing DNA to come closer to the surface.
673 Experimentally, the formation of a stable DX coating of the MNPs was verified at all the examined
674 ionic strength levels. The weaker association between DNA and DX (compared to that between
675 the MNPs and DX) was also attested by the experimental results, since part of DNA was found to
676 be present in its free form, as was predicted by the simulations. Both, in the absence and in the
677 presence of the MNPS, the DNA-DX complexation was found to be enhanced by the presence of
678 salt, which is consistent with the mechanism described by the simulations, regarding the increase
679 of hydrogen bonding between the two moieties upon increasing the ionic strength. In the presence

of the MNPs, the physical adsorption of the DX layer onto the magnetic surface provided a more stable substrate upon which DNA could be adsorbed, decreasing thus further the detection of DNA in its uncomlpexed form.

6. Conclusions

The present work examined the interfacial interactions of DX-coated MNPs with DNA at physiologically relevant conditions, aiming to elucidate their potential use as effective nanocarriers for gene delivery purposes.

The combination of all-atom Molecular Dynamics simulations with experimental data, highlighted the significant role of the polymer coating on the surface of the MNPs in their DNA binding capacity, through a detailed analysis of the energetics and the number of hydrogen bonds formed between the polymer coating and the DNA strands.

The presence of very weak DNA/magnetic surface interactions in the uncoated MNPs, resulted in a transient/unstable binding of DNA. In contrast, DNA binding was much stronger on the DX-coated MNPs. The effects of ionic strength were found to be associated with a more effective DX-DNA binding through the increase of the degree of hydrogen bonding between the two moieties. The ability of DX to interact favorably both with the magnetite surface and with DNA allowed this polysaccharide to act as a mediator for the effective DNA complexation onto the coated NP surface.

The above results show that an effective DNA complexation using MNPs can be realized, by tuning the attraction mechanisms and the binding stability through appropriate particle coating and ionic strength regulation. Based on these findings, further enhancement of the energetic stability of the magnetite-DX-DNA complexes can be sought by appropriate modification of the iron oxide surface, e.g., through the partial hydrogenation of the superficial magnetite oxygens in order to increase the hydrogen bonding interactions between DX and the MNP surface.[62] In addition, an enhancement of the degree of hydrogen bonding between DX and DNA (e.g., by introducing additional hydrogen-bonding-capable-sites in the DX structure) would also be another route towards a more stable DNA complexation.

To summarize, this work provided insights into the mechanism of interaction of biomolecules, such as DNA, with a well-known and clinically approved magnetic carrier, i.e., dextran-coated

Fe_3O_4 nanoparticles. The detailed information obtained through the present combined computational and experimental study may serve as a basis for the development of new improved hybrid gene delivery systems.

AUTHOR INFORMATION

Corresponding Author

***Anastasia Rissanou (A. R.)** –Theoretical & Physical Chemistry Institute, National Hellenic Research Foundation, 48 Vassileos Constantinou Avenue, 11635 Athens, Greece

Authors

Maria Psarrou (M. P.) –Department of Materials Science and Technology, University of Crete, 700 13 Heraklion, Crete, Greece and Institute of Electronic Structure and Laser, FORTH, 700 13 Heraklion, Crete, Greece.

Maria Vamvakaki (M. V.)– Department of Materials Science and Technology, University of Crete, 700 13 Heraklion, Crete, Greece and Institute of Electronic Structure and Laser, FORTH, 700 13 Heraklion, Crete, Greece.

Kostas Karatasos (K. K)– Department of Chemical Engineering, University of Thessaloniki, P.O. BOX 420, 54124 Thessaloniki, Greece.

Author Contributions

Conceptualization, A.R., K.K., M.V.; Methodology, A.R. K.K.; Execution of experiments, M. P.; Data analysis, A.R., M. P.; Validation of results A.R., K. K., M. V., M. P.; writing—original draft preparation, A.R., M. P. All authors have read and agreed to the published version of the manuscript.

Acknowledgements

The authors would like to thank the support of this work by computational time granted from Greek Research & Technology Network (GRNET) in the National HPC facility—ARIS for the Project: Peptide-Graphene nanocomposites though Molecular Simulations, BIOGRAPH. The authors also

acknowledge the use of computational resources of the High-Performance Computing Infrastructure of the Aristotle University of Thessaloniki (AUTh).

Funding Sources

Notes

The authors declare no competing financial interest.

References

1. Shahryari, A.; Saghaeian Jazi, M.; Mohammadi, S.; Razavi Nikoo, H.; Nazari, Z.; Hosseini, E. S.; Burtscher, I.; Mowla, S. J.; Lickert, H., Development and Clinical Translation of Approved Gene Therapy Products for Genetic Disorders. *Frontiers in Genetics* **2019,** *10*.
2. Mendes, B. B.; Conniot, J.; Avital, A.; Yao, D.; Jiang, X.; Zhou, X.; Sharf-Pauker, N.; Xiao, Y.; Adir, O.; Liang, H.; Shi, J.; Schroeder, A.; Conde, J., Nanodelivery of nucleic acids. *Nature Reviews Methods Primers* **2022,** *2* (1), 24.
3. Ramamoorth, M.; Narvekar, A., Non viral vectors in gene therapy- an overview. *J Clin Diagn Res* **2015,** *9* (1), Ge01-6.
4. Pandey, A. P.; Sawant, K. K., Polyethylenimine: A versatile, multifunctional non-viral vector for nucleic acid delivery. *Materials Science and Engineering: C* **2016,** *68*, 904-918.
5. Wu, T.; Li, Z.; Zhang, Y.; Ji, J.; Huang, Y.; Yuan, H.; Feng, F.; Schanze, K. S., Remarkable Amplification of Polyethylenimine-Mediated Gene Delivery Using Cationic Poly(phenylene ethynylene)s as Photosensitizers. *ACS Applied Materials & Interfaces* **2018,** *10* (29), 24421-24430.
6. Patel, A. K.; Kaczmarek, J. C.; Bose, S.; Kauffman, K. J.; Mir, F.; Heartlein, M. W.; DeRosa, F.; Langer, R.; Anderson, D. G., Inhaled Nanoformulated mRNA Polyplexes for Protein Production in Lung Epithelium. *Advanced Materials* **2019,** *31* (8), 1805116.
7. Wen, Y.; Tan, Z.; Sun, F.; Sheng, L.; Zhang, X.; Yao, F., Synthesis and characterization of quaternized carboxymethyl chitosan/poly(amidoamine) dendrimer core–shell nanoparticles. *Materials Science and Engineering: C* **2012,** *32* (7), 2026-2036.
8. Georgiou, T. K.; Vamvakaki, M.; Patrickios, C. S.; Yamasaki, E. N.; Phylactou, L. A., Nanoscopic Cationic Methacrylate Star Homopolymers: Synthesis by Group Transfer Polymerization, Characterization and Evaluation as Transfection Reagents. *Biomacromolecules* **2004,** *5* (6), 2221-2229.
9. Kowalski, P. S.; Rudra, A.; Miao, L.; Anderson, D. G., Delivering the Messenger: Advances in Technologies for Therapeutic mRNA Delivery. *Mol Ther* **2019,** *27* (4), 710-728.
10. Sun, X.; Zhang, N., Cationic Polymer Optimization for Efficient Gene Delivery. *Mini Reviews in Medicinal Chemistry* **2010,** *10* (2), 108-125.
11. Macklin, M. D.; Drape, R. J.; Swain, W. F., Preparations for Particle-Mediated Gene Transfer Using the Accell® Gene Gun. In *DNA Vaccines: Methods and Protocols*, Lowrie, D. B.; Whalen, R. G., Eds. Humana Press: Totowa, NJ, 2000; pp 297-303.

12. Hughes, G. A., Nanostructure-mediated drug delivery. *Nanomedicine: Nanotechnology, Biology and Medicine* **2005,** *1* (1), 22-30.
13. Carvalho, A. M.; Cordeiro, R. A.; Faneca, H., Silica-Based Gene Delivery Systems: From Design to Therapeutic Applications. *Pharmaceutics* **2020,** *12* (7).
14. Okoampah, E.; Mao, Y.; Yang, S.; Sun, S.; Zhou, C., Gold nanoparticles–biomembrane interactions: From fundamental to simulation. *Colloids and Surfaces B: Biointerfaces* **2020,** *196*, 111312.
15. Hosseini, F.; Panahifar, A.; Adeli, M.; Amiri, H.; Lascialfari, A.; Orsini, F.; Doschak, M. R.; Mahmoudi, M., Synthesis of pseudopolyrotaxanes-coated Superparamagnetic Iron Oxide Nanoparticles as new MRI contrast agent. *Colloids and Surfaces B: Biointerfaces* **2013,** *103*, 652-657.
16. Sung, Y. K.; Kim, S. W., Recent advances in the development of gene delivery systems. *Biomaterials Research* **2019,** *23* (1), 8.
17. Sizikov, A. A.; Nikitin, P. I.; Nikitin, M. P., Magnetofection In Vivo by Nanomagnetic Carriers Systemically Administered into the Bloodstream. *Pharmaceutics* **2021,** *13* (11).
18. Farinha, P.; Coelho, J. M. P.; Reis, C. P.; Gaspar, M. M., A Comprehensive Updated Review on Magnetic Nanoparticles in Diagnostics. *Nanomaterials (Basel)* **2021,** *11* (12).
19. Bilal, M.; Iqbal, H. M. N.; Adil, S. F.; Shaik, M. R.; Abdelgawad, A.; Hatshan, M. R.; Khan, M., Surface-coated magnetic nanostructured materials for robust bio-catalysis and biomedical applications-A review. *J Adv Res* **2022,** *38*, 157-177.
20. Zhu, Q.; Chua, M. H.; Ong, P. J.; Cheng Lee, J. J.; Le Osmund Chin, K.; Wang, S.; Kai, D.; Ji, R.; Kong, J.; Dong, Z.; Xu, J.; Loh, X. J., Recent advances in nanotechnology-based functional coatings for the built environment. *Materials Today Advances* **2022,** *15*, 100270.
21. Luo, D.; Wu, C.; Yan, M., Incorporation of the Fe3O4 and SiO2 nanoparticles in epoxy-modified silicone resin as the coating for soft magnetic composites with enhanced performance. *Journal of Magnetism and Magnetic Materials* **2018,** *452*, 5-9.
22. Baki, A.; Wiekhorst, F.; Bleul, R., Advances in Magnetic Nanoparticles Engineering for Biomedical Applications-A Review. *Bioengineering (Basel)* **2021,** *8* (10).
23. Jabeen, N.; Atif, M., Polysaccharides based biopolymers for biomedical applications: A review. *Polymers for Advanced Technologies* **2024,** *35* (1), e6203.
24. Sohrabijam, Z.; Saeidifar, M.; Zamanian, A., Enhancement of magnetofection efficiency using chitosan coated superparamagnetic iron oxide nanoparticles and calf thymus DNA. *Colloids and Surfaces B: Biointerfaces* **2017,** *152*, 169-175.
25. Barclay, T. G.; Day, C. M.; Petrovsky, N.; Garg, S., Review of polysaccharide particle-based functional drug delivery. *Carbohydr Polym* **2019,** *221*, 94-112.
26. Adamczyk-Grochala, J.; Lewinska, A., Nano-Based Theranostic Tools for the Detection and Elimination of Senescent Cells. *Cells* **2020,** *9* (12), 2659.
27. Dias, A. M. G. C.; Hussain, A.; Marcos, A. S.; Roque, A. C. A., A biotechnological perspective on the application of iron oxide magnetic colloids modified with polysaccharides. *Biotechnology Advances* **2011,** *29* (1), 142-155.
28. Abarca-Cabrera, L.; Fraga-García, P.; Berensmeier, S., Bio-nano interactions: binding proteins, polysaccharides, lipids and nucleic acids onto magnetic nanoparticles. *Biomaterials Research* **2021,** *25* (1), 12.
29. Gil, M. H.; Research, S., *Carbohydrates applications in medicine*. Research Signpost Trivandrum, Kerala, India: Trivandrum, Kerala, India, 2014.
30. Psarrou, M.; Mitraki, A.; Vamvakaki, M.; Kokotidou, C., Stimuli-Responsive Polysaccharide Hydrogels and Their Composites for Wound Healing Applications. *Polymers* **2023,** *15* (4), 986.
31. Chircov, C.; Ștefan, R.-E.; Dolete, G.; Andrei, A.; Holban, A. M.; Oprea, O.-C.; Vasile, B. S.; Neacșu, I. A.; Tihăuan, B., Dextran-Coated Iron Oxide Nanoparticles Loaded with Curcumin for Antimicrobial Therapies. *Pharmaceutics* **2022,** *14* (5), 1057.

32. Peng, M.; Li, H.; Luo, Z.; Kong, J.; Wan, Y.; Zheng, L.; Zhang, Q.; Niu, H.; Vermorken, A.; Van de Ven, W.; Chen, C.; Zhang, X.; Li, F.; Guo, L.; Cui, Y., Dextran-coated superparamagnetic nanoparticles as potential cancer drug carriers in vivo. *Nanoscale* **2015,** *7* (25), 11155-11162.
33. Remya, N. S.; Syama, S.; Sabareeswaran, A.; Mohanan, P. V., Toxicity, toxicokinetics and biodistribution of dextran stabilized Iron oxide Nanoparticles for biomedical applications. *International Journal of Pharmaceutics* **2016,** *511* (1), 586-598.
34. Yoo, B.; Ghosh, S. K.; Kumar, M.; Moore, A.; Yigit, M. V.; Medarova, Z., Design of nanodrugs for miRNA targeting in tumor cells. *J Biomed Nanotechnol* **2014,** *10* (6), 1114-22.
35. Wang, Z.; Zeng, X.; Deng, Y.; He, N.; Wang, Q.; Huang, J., Molecular Dynamics Simulations of End-Tethered Single-Stranded DNA Probes on a Silica Surface. *Journal of nanoscience and nanotechnology* **2011,** *11*, 8457-68.
36. Hinkle, K. R., Molecular dynamics simulations reveal single-stranded DNA (ssDNA) forms ordered structures upon adsorbing onto single-walled carbon nanotubes (SWCNT). *Colloids and Surfaces B: Biointerfaces* **2022,** *212*, 112343.
37. Lucas, R.; Gómez-Pinto, I.; Aviñó, A.; Reina, J. J.; Eritja, R.; González, C.; Morales, J. C., Highly polar carbohydrates stack onto DNA duplexes via CH/π interactions. *J Am Chem Soc* **2011,** *133* (6), 1909-16.
38. Rebek, J., Jr.; Askew, B.; Ballester, P.; Buhr, C.; Jones, S.; Nemeth, D.; Williams, K., Molecular recognition: hydrogen bonding and stacking interactions stabilize a model for nucleic acid structure. *Journal of the American Chemical Society* **1987,** *109* (16), 5033-5035.
39. Vacas, T.; Corzana, F.; Jiménez-Osés, G.; González, C.; Gómez, A. M.; Bastida, A.; Revuelta, J.; Asensio, J. L., Role of Aromatic Rings in the Molecular Recognition of Aminoglycoside Antibiotics: Implications for Drug Design. *Journal of the American Chemical Society* **2010,** *132* (34), 12074-12090.
40. Newcomb, L. F.; Gellman, S. H., Aromatic Stacking Interactions in Aqueous Solution: Evidence That neither Classical Hydrophobic Effects nor Dispersion Forces Are Important. *Journal of the American Chemical Society* **1994,** *116* (11), 4993-4994.
41. Shi, J.-H.; Liu, T.-T.; Jiang, M.; Chen, J.; Wang, Q., Characterization of interaction of calf thymus DNA with gefitinib: Spectroscopic methods and molecular docking. *Journal of Photochemistry and Photobiology B: Biology* **2015,** *147*, 47-55.
42. Beenackers, J. A. W. M.; F.M. Kuster, B.; van der Baan, H. S., Ionisation and solvation of d-glucose. *Carbohydrate Research* **1985,** *140* (2), 169-183.
43. Bhattacharyya, L.; Rohrer, J. S., Appendix 2: Dissociation Constants (pKa) of Common Sugars and Alcohols. *Applications of Ion Chromatography for Pharmaceutical and Biological Products* **2012**, 455-456.
44. Desbrieres, J.; Peptu, C. A.; Savin, C. L.; Popa, M., 10 - Chemically Modified Polysaccharides With Applications in Nanomedicine. In *Biomass as Renewable Raw Material to Obtain Bioproducts of High-Tech Value*, Popa, V.; Volf, I., Eds. Elsevier: 2018; pp 351-399.
45. Gómez Pérez, A.; González-Martínez, E.; Díaz Águila, C. R.; González-Martínez, D. A.; González Ruiz, G.; García Artalejo, A.; Yee-Madeira, H., Chitosan-coated magnetic iron oxide nanoparticles for DNA and rhEGF separation. *Colloids and Surfaces A: Physicochemical and Engineering Aspects* **2020,** *591*, 124500.
46. Bragg, W. H., The Structure of Magnetite and the Spinels. *Nature* **1915,** *95* (2386), 561-561.
47. Tsave, O.; Psarrou, M.; Kastrinaki, G.; Papachristou, E.; Papi, R.; Zaspalis, V.; Nalbandian, L.; Sarafidis, C.; Choli-Papadopoulou, T.; Vamvakaki, M.; Chatzidoukas, C., Functional polysaccharide-coated SPIONs for in vitro mRNA delivery in breast cancer cells. *Materials Advances* **2024,** *5* (13), 5410-5432.
48. Ardizzone, S.; Biagiotti, R.; Formaro, L., A Reexamination of the point of zero charge of magnetite in aqueous solutions. *Journal of Electroanalytical Chemistry and Interfacial Electrochemistry* **1982,** *135* (1), 167-172.

49. Astumian, R. D.; Sasaki, M.; Yasunaga, T.; Schelly, Z. A., Proton adsorption-desorption kinetics on iron oxides in aqueous suspensions, using the pressure-jump method. *The Journal of Physical Chemistry* **1981,** *85* (25), 3832-3835.
50. Tombácz, E.; Majzik, A.; Horvát, Z.; Illés, E., Magnetite in aqueous medium: Coating its surface and surface coated with it. *Romanian Reports in Physics* **2006,** *58*, 281-286.
51. Park, H.; May, A.; Portilla, L.; Dietrich, H.; Münch, F.; Rejek, T.; Sarcletti, M.; Banspach, L.; Zahn, D.; Halik, M., Magnetite nanoparticles as efficient materials for removal of glyphosate from water. *Nature Sustainability* **2020,** *3*, 129-135.
52. Hess, B.; Kutzner, C.; van der Spoel, D.; Lindahl, E., GROMACS 4: Algorithms for Highly Efficient, Load-Balanced, and Scalable Molecular Simulation. *J Chem Theory Comput* **2008,** *4* (3), 435-447.
53. Huang, J.; MacKerell, A. D., Jr., CHARMM36 all-atom additive protein force field: validation based on comparison to NMR data. *J Comput Chem* **2013,** *34* (25), 2135-45.
54. Huang, J.; Rauscher, S.; Nawrocki, G.; Ran, T.; Feig, M.; de Groot, B. L.; Grubmüller, H.; MacKerell, A. D., Jr., CHARMM36m: an improved force field for folded and intrinsically disordered proteins. *Nat. Methods* **2017,** *14* (1), 71-73.
55. Denning, E. J.; Priyakumar, U. D.; Nilsson, L.; Mackerell, A. D., Jr., Impact of 2'-hydroxyl sampling on the conformational properties of RNA: update of the CHARMM all-atom additive force field for RNA. *Journal of computational chemistry* **2011,** *32* (9), 1929-43.
56. Jorgensen, W. L.; Chandrasekhar, J.; Madura, J. D.; Impey, R. W.; Klein, M. L., Comparison of simple potential functions for simulating liquid water. *The Journal of Chemical Physics* **1983,** *79* (2), 926-935.
57. Bussi, G.; Donadio, D.; Parrinello, M., Canonical sampling through velocity rescaling. *J. Chem. Phys.* **2007,** *126* (1), 014101.
58. Liu, B.; Poolman, B.; Boersma, A. J., Ionic Strength Sensing in Living Cells. *ACS chemical biology* **2017,** *12* (10), 2510-2514.
59. Dickerhoff, J.; Appel, B.; Müller, S.; Weisz, K., Sugar–Edge Interactions in a DNA–RNA G-Quadruplex: Evidence of Sequential C–H···O Hydrogen Bonds Contributing to RNA Quadruplex Folding. *Angewandte Chemie International Edition* **2016,** *55* (48), 15162-15165.
60. Haase, L.; Karg, B.; Weisz, K., Manipulating DNA G-Quadruplex Structures by Using Guanosine Analogues. *ChemBioChem* **2019,** *20* (8), 985-993.
61. Qiang, L.; Yang, T.; Li, Z.; Wang, H.; Chen, X.; Cui, X., Molecular dynamics simulations of the interaction between Fe3O4 and biocompatible polymer. *Colloids and Surfaces A: Physicochemical and Engineering Aspects* **2014,** *456*, 62–66.
62. Schwarz, F.; Pomp, S.; Seidel, P.; Li, X.; Paier, J.; Sterrer, M., Hydrogen-bond-stabilized high density catechol monolayer on magnetite Fe3O4(111). *Surface Science* **2022,** *719*, 122027.